GeoScienceWorld
Lithosphere
Volume 2022, Article ID 6405238, 14 pages
https://doi.org/10.2113/2022/6405238

Lithosphere

Research Article

Provenance Discrimination of Siliciclastic Sediments in the Western Sea of Japan over the Past 30 kyr: Evidence from Major, Trace Elements, and Pb Isotopes

Ruxi Dou,[1,2,3] **Jianjun Zou**,[2,4] **Xuefa Shi**,[2,4] **Aimei Zhu**,[2,4] **Zhi Dong**,[2] **Xinqing Zou**,[1,3] **and Serge Gorbarenko**[5]

[1]*Collaborative Innovation Center of South China Sea Studies, Nanjing University, Nanjing 210093, China*
[2]*Key Laboratory of Marine Geology and Metallogeny, First Institute of Oceanography, Ministry of Natural Resources, Qingdao 266061, China*
[3]*School of Geographic and Oceanographic Sciences, Ministry of Education Key Laboratory for Coast and Island Development, Nanjing University, Nanjing 210093, China*
[4]*Laboratory for Marine Geology, Pilot National Laboratory for Marine Science and Technology (Qingdao), Qingdao 266237, China*
[5]*V.I. Il'ichev Pacific Oceanological Institute, Far East Branch of the Russian Academy of Sciences, Vladivostok 690041, Russia*

Correspondence should be addressed to Xuefa Shi; xfshi@fio.org.cn and Xinqing Zou; zouxq@nju.edu.cn

Received 19 January 2022; Accepted 2 June 2022; Published 27 June 2022

Academic Editor: Hema Achyuth

The Sea of Japan (JS), a unique marginal sea without any large river influxes in the western Pacific, provides ample information about the evolution of sea level, East Asian monsoons (EAM), sea ice activity, and ocean currents in geological time. However, insufficient investigation in the western JS limits our knowledge of East Asian climate change. This study utilizes major and trace elements and Pb isotopes of fine siliciclastic components (<63 μm) of core LV53-18-2 and determines the provenances using statistical methods and discrimination diagrams. The results show that the terrigenous debris of LV53-18-2 was mainly composed of aeolian dust from northeast China, ice-rafted debris (IRD), and volcanic materials from the Far East coast over the last 30 kyr. During the late last glacial period, sea ice activity carried weakly weathered IRD to the study area. Meanwhile, the strengthened East Asian winter monsoon (EAWM) brought dust from northeast China to the study site owing to the cold climate and enlarged sandy land. During the late last deglacial period to early Holocene (15-8 kyr), ascending boreal summer insolation drove the intense melting of sea ice. This led to the deposition of large amounts of weakly weathered IRD and remarkably influenced the chemical composition of the core. After 8 kyr, the global sea level rose to -15 m below the modern sea level and opened the Tatar Strait. Consequently, freshwater supplied by the Amur River entered the JS and gave birth to the Liman Cold Current (LCC), which transported more mafic materials from the Kema terrane upstream.

1. Introduction

Marine sediments are characterized by older records, expansive sampling areas, and better preservation [1]. Marginal seas act as pivots of materials and energy communication between continents and oceans and receive abundant detrital input with high sediment rates, making it possible to reconstruct paleoclimatic evolution and processes with higher resolution [2].

Among the marginal seas of the Pacific, the Sea of Japan is unique in providing insights into the climatic and environmental evolution of East Asia in the past [3]. The JS communicates with adjacent seas through four shallow straits (Figure 1). The Tsushima Warm Current (TWC), a branch of the Kuroshio Current, enters the JS via its deepest straits (Tsushima Strait, ~130 m) from the south, affecting its oceanography by supplying vast amounts of heat and saline [3]. Consequently, the paleoceanographic evolution of the JS

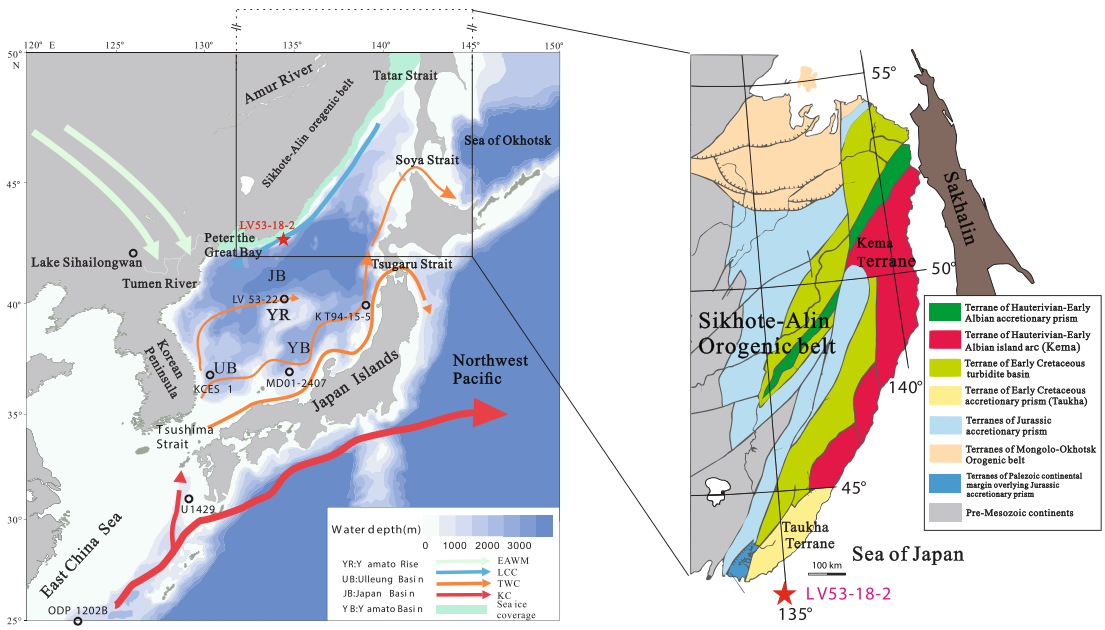

FIGURE 1: Location of sediment core LV53-18-2 in this study and geologic scheme of the Sikhote-Alin region (modified from [45, 66]). Other cores are shown for reference; core Lake Sihailongwan is from [47]; cores ODP 1202B and U1429 in Okinawa Trough are from [20, 67]; cores LV53-22, KT94-15-5, MD01-2407, and KCES-1 come from [5–7, 9], respectively.

changed dramatically throughout the Quaternary, when the sea level fluctuated periodically [4]. The westerly jet (WJ) and East Asia winter monsoon (EAWM) bring dust from the Taklimakan Desert and the Mongolian Gobi Desert to the JS, which are mainly regulated by dry-wet conditions in the East Asian interior [5, 6]. Currently, no large rivers flow into the JS, resulting in a limited terrigenous supply from the neighboring landmass and a significant difference in sedimentation patterns from other marginal seas [7–9].

Previous studies have revealed that thick sediments in the JS archived tectonic framework changes in East Asia, the growth and decay of global ice volume [10, 11], and light-dark laminated layers that record East Asia summer monsoon (EASM) oscillations and current intrusion at millennial timescale [3, 12]. A series of progress has been made concerning the provenance research of the JS, employing sedimentology, mineralogy, and elemental geochemistry. These studies show that the sediments in the central part of the JS since the Miocene are mainly a mixture of central Asian aeolian dust and riverine input from the island arc [10]. The properties of terrestrial components in the JS are heterogeneous, with dominant continental clasts in the central and southern JS, but prominent mafic contributions in the western JS [8, 9]. Overall, provenance research since the last glacial period in the central and southern parts of the JS is sufficient. However, the investigations in the western and northern regions are very scarce, which limits our comprehensive understanding of the basin-wide paleoenvironment evolution of the JS.

There are many processes from sediments generation to deposition, including physical and chemical weathering, dynamic sorting, and resuspension after deposition. These processes eventually lead to grain size, mineral composition, elemental composition, and isotopic geochemical changes [13]. As an essential aspect of paleoclimatic and paleoenvironmental research, provenance studies have focused on changes in stable constituents in sediments, such as weathering-resistant minerals, stable elements, and isotopes [14]. High-field strength elements tend to crystallize in magma and are averse to weathering. Therefore, they have the potential to distinguish and trace the source area of terrigenous components, thus acting a powerful tool for reconstructing the paleoenvironment. Sr-Nd-Pb isotopes are the most commonly used isotope combinations for provenance tracing. Sr isotopes are typically used in pairs with Nd because of grain size effects [15–17]. Although the relationship between Pb isotopes and grain size has not been clearly established, many applications have proven its reliability in source tracing [18–20].

This study presents minor elements, and Pb isotope records the core LV53-18-2 in the western JS. Combined with the published Nd data of this core [8], this study makes further efforts to reconstruct changes in sediment provenance and discuss the main controlling factors, aiming to provide a better explanation of the paleoenvironmental evolution in the western JS over the last 30 kyr.

2. Geological and Oceanographic Settings

Geologically, the JS is a back-arc basin lying on the southeastern part of the Amur plate, which includes the Korean Peninsula, Japan arc, northeastern China, and Russian Far East. The opening of the JS occurred in the early Miocene and was controlled by large intracontinental strike-slip faults. The major plate reorganization in East Asia in the Early Middle Miocene (ca. 15 Ma) led to the JS back-arc closure that continues today [21]. The JS is a semi-enclosed marginal sea, spanning from the subtropical to the subpolar

zone (Figure 1), covering one million square kilometers and has an average depth of 1650 m. The JS is composed of the Ulleung Basin, Yamato Basin, and Japan Basin, and exchanges water with the East China Sea, Pacific Ocean, and Sea of Okhotsk via four straits: Tsushima Strait (130 m), Tsugaru Strait (130 m), Soya Strait (55 m), and Tatar Strait (15 m) from the south to north [22].

At present, the surface of the JS is covered by counterclockwise surface circulation, which is mainly composed of the southern TWC and the northern Liman Cold Current (LCC), dominating the surface hydrology of the JS [23]. The TWC is presently the only current flowing into the JS. It is formed after a branch of the Kuroshio Current mixes with freshwater input from the Changjiang River (Yangtze River) in the East China Sea and carries a large amount of water with heat and saline to the JS [24]. After entering the JS, the TWC divides into three branches. The first and second branches flow northeastward along the western side of the Japanese island. The third branch flows northward along the eastern edge of the Korean Peninsula and then turns east, crossing the middle of the JS at approximately 38°N [25]. A subpolar front is generated when the TWC mixes with cold northern water [26]. Seasonal sea ice forms in the northern part of the JS in winter, mainly in the Tatar Strait, the coast of the Far East, and Peter the Great Bay. It has been suggested that the formation of seasonal sea ice is related to the frequency of storm occurrence and intensity of the EAWM [27]. The melting of sea ice in late spring and summer, accompanied by the input of freshwater from the Amur River, gives rise to the LCC [28].

The JS is one of the few areas where deep water circulation has developed in modern times [29, 30]. The nature of water below 300 m is homogeneous, characterized by low temperature, high salinity, and high dissolved oxygen, and is called Japan Sea Proper Water (JSPW) [31]. Studies have proven that brine rejection related to the formation of sea ice in winter in the western JS contributes to the generation of the JSPW. Compared with other seas, the JSPW has a very short residence time (approximately 100 years) and is sensitive to climate and environmental change [32]. Previous studies have shown that since the 1950s, the oxygen content of the JSPW has significantly reduced, and the water structure has changed, which both could influence the marine fisheries and ecosystems of JS [33].

3. Materials and Methods

A 393 cm long sediment core LV53-18-2 (42° 56′ N, 134° 44′ E, 551 m depth) was retrieved from the western slope of the JS during the first China-Russia joint cruise in 2010 (Figure 1). This core was composed of grayish green to grayish brown fine silt. Owing to lack of sufficient foraminifera to conduct radiocarbon dating, 7 optically stimulated luminescence (OSL) samples were used to establish the age model of LV53-18-2 (Table 1). Preparation and luminescence measurements were performed at the Luminescence Dating Laboratory of the Nanjing Institute of Geography and Limnology, Chinese Academy of Sciences, China. The samples for dating were wet sieved to obtain a fraction of <38 μm and treated with 10% HCl and 30% H_2O_2 to remove organic components and carbonates. The residual fraction was separated according to Stokes' law and etched in 30% H_2SiF_6 to obtain pure quartz for OSL dating. More details about these procedures are provided in [34]. The age of the bottom layer was determined to be 30.02 ± 1.66 kyr.

Table 1: Age model of core LV53-18-2 according to OSL data.

Core	Depth (cm)	OSL age (ka)	Error (ka)
LV53-18-2	82	7.11	±0.41
LV53-18-2	153	14.97	±0.84
LV53-18-2	193	18.91	±1.01
LV53-18-2	217	21.60	±1.12
LV53-18-2	292	24.18	±1.3
LV53-18-2	317	26.27	±1.47
LV53-18-2	393	30.02	±1.66

The core was subsampled at a 1-cm interval. A total of 120 samples were chosen for elemental measurement. Twenty-eight samples were used for the Pb isotopic measurements at the Key Laboratory of Marine Geology and Metallogeny, First Institute of Oceanography, Ministry of Natural Resources, China. Preparations, including wet sieving, carbonates, and organic removal, were conducted to obtain a <63 μm silicate component. For elemental measurement, approximately 50.00 mg of powdered sample was digested entirely in a mixture of ultrapure HNO_3-HF-HCl in a Teflon beaker. Major and trace elements were analyzed using inductively coupled plasma optical emission spectroscopy (ICP-OES; Thermo Scientific iCAP 6000, Thermo Fisher Scientific) and inductively coupled plasma mass spectrometry (ICP-MS; Thermo Scientific X-SERIES 2, Thermo Fisher Scientific), respectively. For quality control, the reference material GSD-9, duplicate, and blank samples were used. All blank samples were below the detection limit, and the relative standard deviations of the major and trace element analyses were <5%.

For Pb isotope measurements, pretreated samples were dissolved using a mixture of ultrapure HNO_3-HF-$HClO_4$ followed by extraction using a column filled with anion exchange resin (AG1-X8). Samples were loaded into the columns as 0.6 M HBr solution. The column was washed twice with 1 ml of 6 M HCl and 1 ml of Milli-Q water and then conditioned with 1 ml of 0.6 N HBr. After loading samples, 0.5 ml of 0.6 N HBr was added to elute three times. Finally, the Pb fractions were collected using 1 ml 6 N of HCl. The Pb isotopic compositions were measured using a Nu plasma multicollector ICP-MS (MC-ICP-MS; Nu Instruments). The Tl-spike method corrected Pb isotope ratios for instrumental mass fractionation and machine bias. Repeated analyses of NIST SRM 981 standard gives $^{208}Pb/^{206}Pb = 36.6863 \pm 0.0008$ (2δ), $^{207}Pb/^{206}Pb = 15.4878 \pm 0.0003$ (2δ), and $^{206}Pb/^{204}Pb = 16.9351 \pm 0.0004$ (2δ).

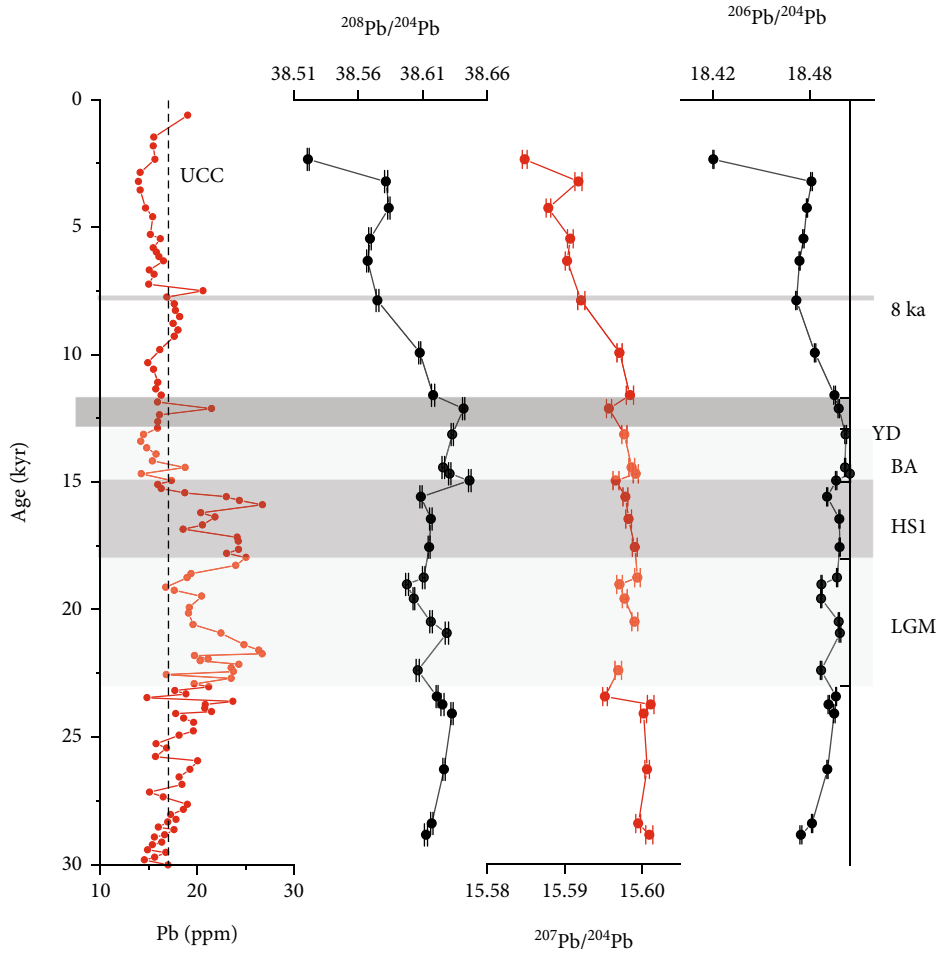

Figure 2: Temporal variations of Pb concentration and its isotopic ratios.

4. Results

4.1. Pb Isotopes. Pb concentrations and isotopic compositions are shown in Figure 2. The Pb concentrations vary from 14.17 to 26.77 ppm. Compared to Pb concentrations in the upper continental crust (UCC) [35], the average value of this core was higher during 30-w15 kyr but was lower after 15 kyr. Values of $^{208}Pb/^{204}Pb$, $^{207}Pb/^{204}Pb$, and $^{206}Pb/^{204}Pb$ fall in the ranges from 38.52107 to 38.64643, 15.58484 to 15.60252, and 18.42027 to 18.50494, respectively. Pb isotopes in the vertical variation show similar patterns, and they all display small fluctuations before 10 kyr and then show a decreasing trend.

4.2. Major and Trace Elements. The underlying hypothesis is that the geochemical data set represents a mixture of different chemical sources. Factor analysis is often used to simplify a large matrix of variables measured on many geochemical samples, identifying relationships between variables in a dataset based on the correlation structure of the variables. To better reveal the control mechanism behind the elements data of LV53-18-2, we used Statistical Product and Service Solutions (SPSS 26, IBM) to perform a Q-mode factor analysis (varimax-rotated) on a dataset of 25 elements, including Al_2O_3, K_2O, TFe_2O_3, MgO, TiO_2, Na_2O, MnO, Sc, V, Cr, Co, Ni, Cu, Zn, Pb, Rb, Ba, Nb, Ta, Th, Zr, Hf, U, and rare earth elements (summed to ∑REE). These elements can be sorted into three factors (Table 2). As is shown in Figure 3, F1 contains Al_2O_3, TFe_2O_3, MgO, TiO_2, Sc, V, Cr, Co, Ni, Cu, Zn, and Pb. Concentrations of these elements before 15 kyr were relatively higher than those after 15 kyr, except for some millennial-scale low values. F2 consists of K_2O, Rb, Ba, Nb, Ta, Th, and ∑REE (Figures 4(a)–4(g)). They displayed a relatively smooth trend from the bottom to 8 kyr, except during HS1. After 8 kyr, the concentration of F2 gradually decreased, in contrast to the increasing trend of most elements in F1. Zr and Hf, members of F3 (Figures 4(h) and 4(i)), had a similar trend to indicators of seasonal sea ice activity, especially during 15-8 kyr (Figures 4(j) and 4(k)).

To further reveal the mechanisms behind the elemental changes, we analyzed the correlation between Al_2O_3 and the partial elements of F1 and F2 (Figures 5 and 6). Al_2O_3 has a good correlation with most elements of F1 and F2 during 30-8 kyr. After 8 kyr, Al_2O_3 still had a moderate correlation with TFe_2O_3, MgO, and Sc, but the coefficients of K_2O, Rb, Th, and Ta were notably reduced, indicating provenance variations after 8 kyr.

Table 2: Matrix of factor loadings (varimax rotation) of sediment geochemical elements in core LV53-18-2.

	Factor1	Factor2	Factor3
MgO	*0.960*	0.203	-0.123
Co	*0.959*	0.041	-0.137
Ni	*0.956*	0.141	-0.172
V	*0.944*	0.213	-0.085
TFe_2O_3	*0.932*	0.218	-0.134
Cu	*0.917*	0.101	-0.253
Cr	*0.877*	-0.110	0.214
Sc	*0.872*	0.361	-0.186
TiO_2	*0.795*	0.293	0.335
Al_2O_3	*0.767*	0.569	-0.059
Zn	*0.746*	0.554	-0.237
Pb	*0.725*	0.539	0.019
Na_2O	-0.620	-0.515	0.471
K_2O	0.183	*0.946*	0.040
Rb	0.245	*0.927*	-0.156
Ta	0.137	*0.921*	0.110
Th	0.336	*0.908*	0.023
Nb	-0.001	*0.880*	0.109
REE	0.188	*0.860*	0.265
Ba	0.212	*0.741*	0.306
U	0.562	0.580	0.130
Hf	-0.499	0.340	*0.726*
Zr	-0.545	0.295	*0.715*
MnO	0.335	-0.394	0.493
Variance (%)	41.71%	35.60%	8.05%
Cumulative variance (%)	41.71%	77.31%	85.36%

5. Discussions

5.1. Potential Terrigenous Sediment End-Members. Using sediment grain size, mineralogy, and geochemistry, previous studies have demonstrated that the East Asian continent and the Japanese archipelago are the two primary sources of terrigenous sediments in the JS [36]; and ocean currents, rivers, EAWM/WJ, and sea ice are all possible transportation agencies [6, 8–10, 37, 38]. Dust from the arid land of East Asia can be carried over the JS by the EAWM/WJ and settled to deposition. Aeolian dust deposition since the middle Miocene has been recognized in the central JS, and it archives information about the strengthened aridification of central Asia, Tibetan uplift, and global cooling [10]. On orbital and millennial timescales, dust records in the southern JS revealed a meridional transition of the WJ, supported by variations in the relative contribution from the Taklamakan Desert and Mongolian Gobi Desert [6].

The Changjiang River (Yangtze River) and Huanghe River (Yellow River) can carry large amounts of suspension into the East China Sea, a portion of which can be delivered into the JS via the Tsushima Strait by the TWC [39]. Sr-Nd isotopes have proved that most of the fine-grain sediments in the southern JS came from East Asia, delivered by the Changjiang River and Huanghe River since the last glacial period; the Changjiang River played a critical role in offering terrestrial materials to the southern JS after 7 kyr [9]. However, no large river flows directly into the JS. The riverine input from small rivers, such as the Nakdong River on the Korean Peninsula, the Tumen River in northeast Asia, and a series of rivers on the Japanese archipelago, is all limited to the coastal area [37, 40].

Sediment core LV53-18-2 was recovered from the western JS, where provenance studies are scarce. Therefore, the geological background of the study area, potential terrigenous supply, and transport forces must be carefully evaluated [8]. The Sikhote-Alin orogenic belt, situated in the Russian Far East, is a potential source area for our core. First, riverine contribution should be neglected because there are no large rivers in this region. The Amur River, which streams into the Sea of Okhotsk and is blocked by the shallow Tatar Strait (15 m), can hardly influence the core composition [3]. Second, there are no records of desertification in this region, which eliminates the possibility of dust sources [41]. Third, seasonal sea ice covers the northern Tatar Strait, the coast of the western JS, and Peter the Great Bay in modern winter [42]. When the climate became colder, the seasonal sea ice would expand southward [43]. Unsorted debris transported by sea ice would settled in the study area when the ice melted. Sea ice activity over the last 30 kyr has been reconstructed with the LV53-18-2 grain size proxy (Figures 4(j) and 4(k)), showing an intense melting period during 15-8 kyr and late LGM. This results in large quantities of IRD deposition [8]. In brief, sea ice and currents are two reasonable transport modes, the source of which remains inexplicit.

Previous studies of the Sikhote-Alin orogenic belt lithology showed two terranes along the coast: the Kema and Taukha terranes. The Kema Terrane is a fragment of the Barremian-Albian island arc system after colliding with the late Albian continental margin and mainly consists of flysch deposits and volcanic-sedimentary rocks [44]. The Taukha Terrane is an Early Cretaceous accretionary prism composed of various materials, including pelagic to hemipelagic, and marginal deposits [45, 46]. In summary, these two terranes are both potential sources for our core, and volcanic components characterize the Kema Terrane. However, the nature of the Taukha Terrane cannot be compared with that of our core because of its complexity [45].

5.2. Elemental and Pb Isotopic Evidence for Provenance Change

5.2.1. Pb Isotopes. Lead isotopes have been used as tracers in sediment provenance studies. Based on previous work, we grouped the Pb isotopes of LV53-18-2 into three intervals. Compared to data before 15 kyr, $^{207}Pb/^{204}Pb$ ($^{206}Pb/^{204}Pb$ and $^{208}Pb/^{204}Pb$) of 15–8 kyr were less (more) radiogenic during 15–8 kyr, indicating source changes induced by the IRD input (Figure 7). After 8 kyr, $^{206}Pb/^{204}Pb$, $^{207}Pb/^{204}Pb$, and $^{208}Pb/^{204}Pb$ ratios decreased remarkably (Figure 7(a)). Compared to the published data of potential sources, our dataset was closer to volcanic material and far from the East

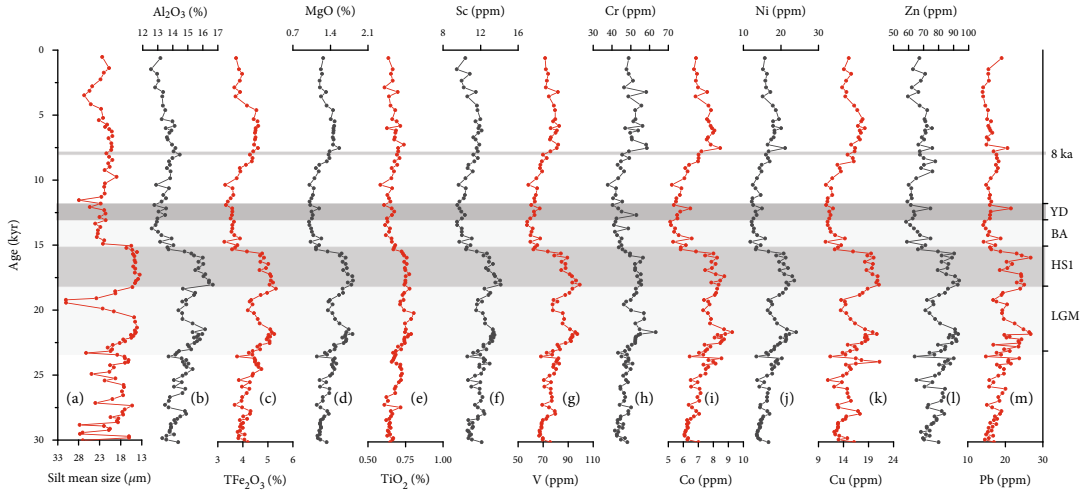

Figure 3: Temporal variations of silt mean size and elements concentration in Factor 1.

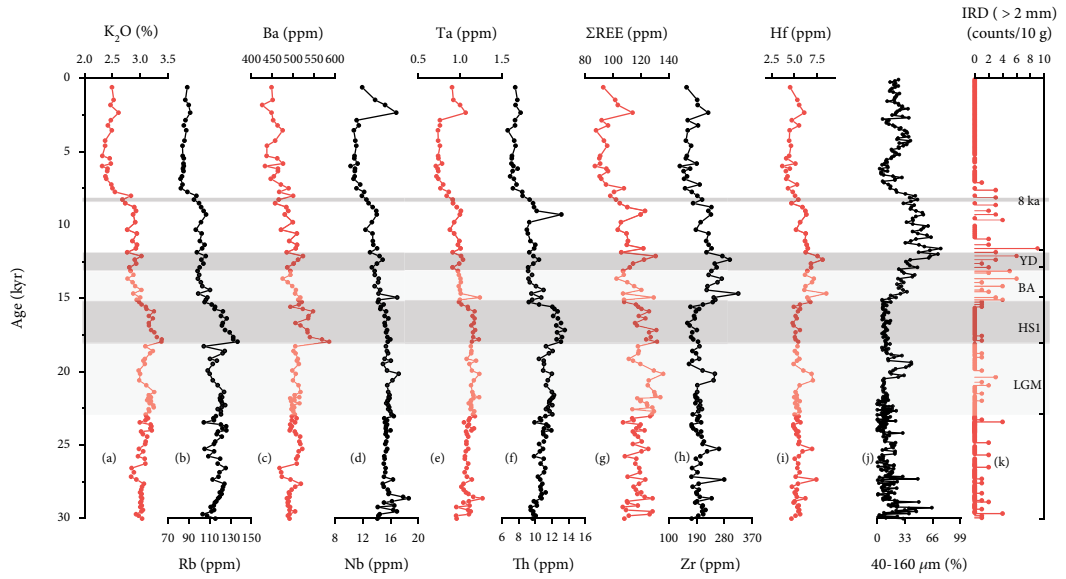

Figure 4: Temporal variations of elements concentration in factors 2 (a–g) and 3 (h–i), and sea ice activity in LV53-18-2 (j–k).

Asian continent represented by the Chinese Loess Plateau, Changjiang River, and Huanghe River (Figures 7(b) and 8). This is consistent with the Sr-Nd isotopes of this core [8], implying the validity of Pb isotope tracing and the large source difference between the central and western JS.

5.2.2. Major and Trace Elements. The concentration of elements in F1 varied inversely to the mean silt size over the last 30 kyr, indicating that the mean grain size (<63 μm) is the main controlling factor of F1 [8] (Figure 3). Elements in F2 were all incompatible and preferred to be enriched in the UCC. Therefore, F2 may represent the input change in continental sourced materials. Specifically, Nb, Ta, Th, and ∑REE are high-field strength elements, which are more weathering resistant and immobile than large ion lithophile elements represented by K, Rb, and Ba. The Zr and Hf in F3 are also high-field strength elements and are usually enriched in heavy minerals. Concentrations of Zr and Hf showed larger values during 15-8 kyr, coincidental with sediment proxies of sea ice activity, indicating that Zr and Hf both can reflect hydrodynamic conditions, and IRD input had influenced sediment components remarkably during 15-8 kyr (Figure 4).

We compared our data with the Kema terrane, northeast China sandy land, UCC, Japan arc, Chinese Loess Plateau, and Mongolian Gobi Desert and drew La-Th-Cr (Figure 9(a)) and La-Th-Sc (Figure 9(b)) ternary plots to discriminate the provenance of our core. These two plots show source changes where continental components (northeast China, UCC, and Chinese Loess) decreased and volcanic materials (Kema terrane and Japan arc) increased from the late last glacial period to the Holocene. The UCC,

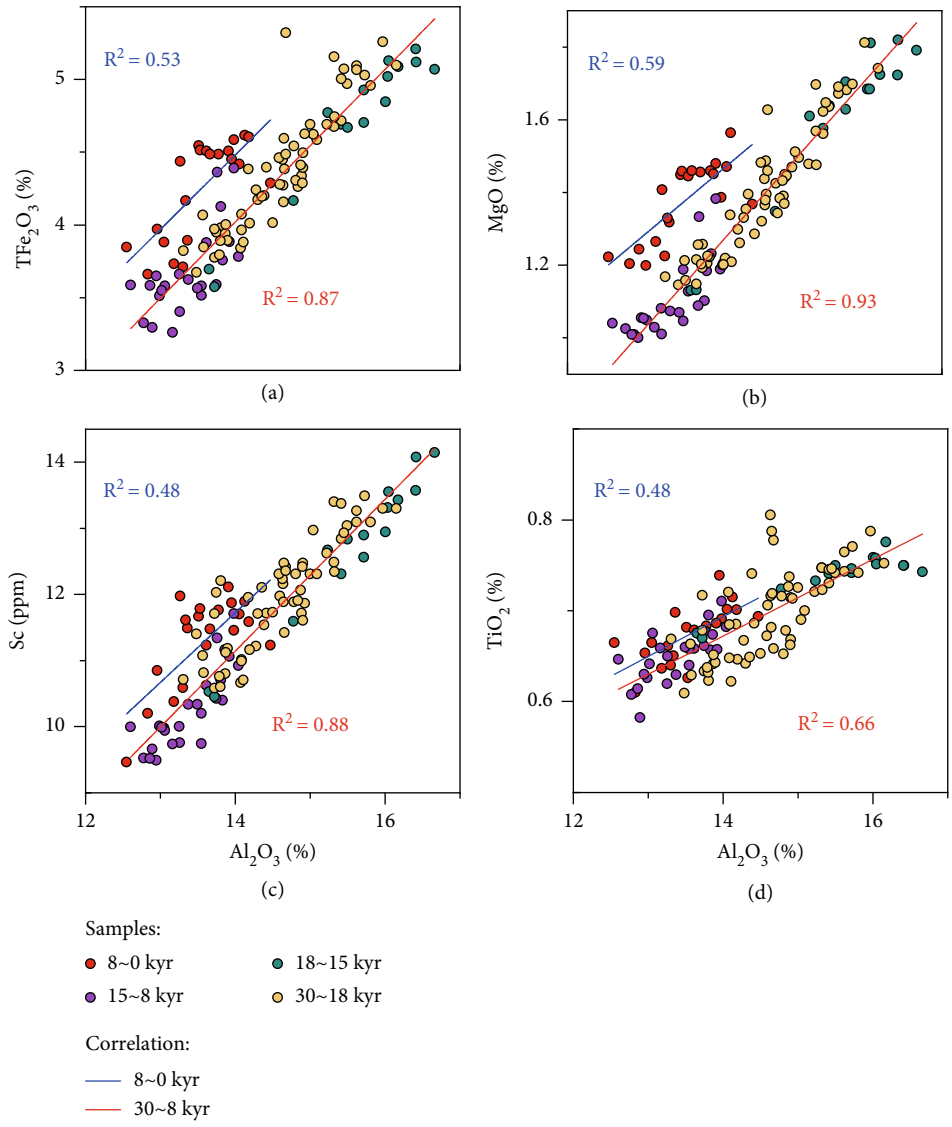

Figure 5: The correlation plot between Al_2O_3 and elements in factor 1.

Taklamakan Desert, and Chinese Loess should be excluded because their Nd and Pb isotopes are very different from those of core LV53-18-2. Therefore, northeast China is a potential source area for western JS aeolian dust. Based on the isotopic Sr-Nd composition of dust in Lake Sihailongwan, northern China (northeast China more precisely) is considered the primary source, and northwesterly winds associated with the EAWM/WJ are carriers of dust from these deserts to the Lake Sihailongwan throughout the past 80 kyr [47]. This conclusion is consistent with our inference that EAWM can transport aeolian dust to the study area [8].

Although both the Japan arc and Kema terrane in the Far East are of volcanic origin, it is more reasonable to recognize the Kema terrane as the main source after 8 kyr than the Japan arc if we consider the geographical location and current direction. In addition, it is worth noting that we have discovered the provenance difference between 15 and 8 kyr with other periods, but were unable to discriminate its source area due to insufficient inference data.

5.3. Paleoenvironmental Evolution in the Western JS since 30 kyr. As mentioned above, our results revealed four-stage variations in elemental compositions and Pb isotopes and recognized northeast China and the Kema terrane as two primary terrigenous sources of core LV53-18-2. We used the Th/Sc ratio to indicate the relative contribution of felsic to mafic source materials [14] and also calculated the chemical index of alteration (CIA) to evaluate chemical weathering in source areas [48]. To reconstruct the paleoenvironmental evolution in the western JS over the last 30 kyr, we compared our elemental proxies with the boreal summer insolation, EASM intensity, global sea level, sea ice activity, and δEu of LV53-18-2 and TWC intensity of LV53-22 in the central JS (Figure 10).

5.3.1. Dust and IRD Input during the Late Last Glacial Period (30~15 kyr). During the late last glacial period, East Asia was characterized by lower boreal insolation [49] (Figure 10(a)), strengthened EAWM [50], and weakened EASM [51]

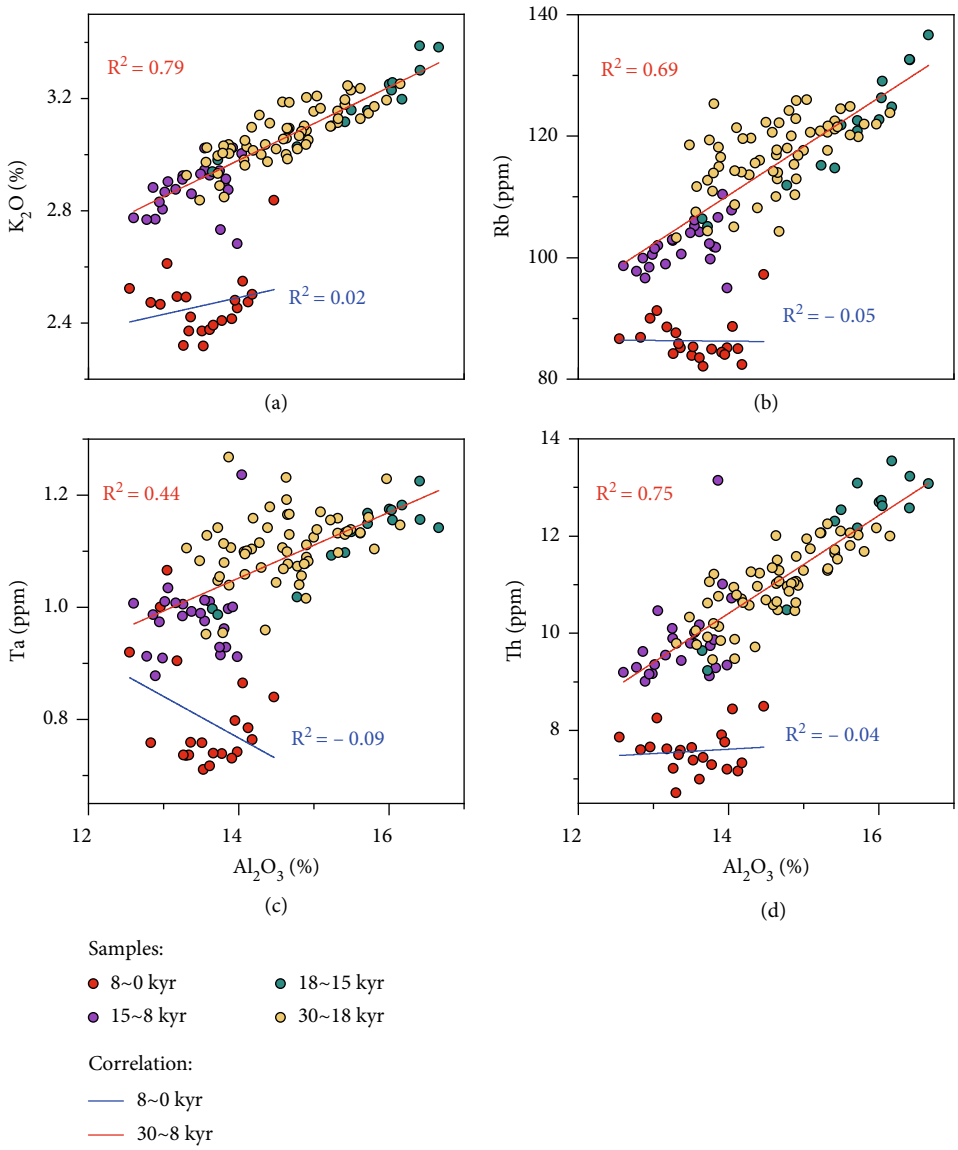

FIGURE 6: The correlation plot between Al_2O_3 and elements in factor 2.

(Figure 10(b)). The JS was nearly closed to open seas when the global sea level dropped to -130 m during the LGM [52] (Figure 10(c)), suppressing the inflow of the TWC and facilitating the stratification of upper water and ventilation deterioration [53–55]. The colder and dryer climates in East Asia induced intensified desertification, with sandy land in northern China expanding to the southeast relative to the Holocene [56]. The enlarged arid area accompanied by enhanced EAWM intensity contributed more dust to the downwind region. The reported three cores that received dust deposition, ODP 797 in the central JS [57], KT94-15-5 in the eastern JS, and MD01-2407 in the southern JS [5] all showed a high flux of dust input during the marine isotope stage 2 (MIS 2). Combined with previous Sr-Nd isotopic evidence and the elemental results in this study [8], we suggest a continuous aeolian input transported by the EAWM from northeast China occurred during the late last glacial period.

Previous research has revealed millennial sea ice activities in the eastern JS since MIS 6 and suggested that this is relevant to the intensity of the EAWM [58]. Our core recorded millennial sea ice activities over the last 30 kyr, including a prominent sea ice melting event at 19 kyr [59] (Figure 10(d)). Synchronously, the TWC taxa and JSPW assemblage of radiolaria in core LV53-23 resumed in the central JS at 19 kyr, indicating an increased intrusion of the TWC [60] (Figure 10(h)). It is recognized that a global warming event may had occurred at 19 kyr, which is synchronized with an increase in greenhouse gas concentrations [61], an abrupt rise in sea level in the East China Sea [62], and a negative excursion of speleothems $\delta^{18}O$ in East Asia [63]. Our results show that the 19 kyr ice melting event in our core may have responded to this sudden hemispheric warming noting that this event cannot be well constrained due to OSL dating error. If this respondence stands, we suggest that the rising sea level may have led the TWC to

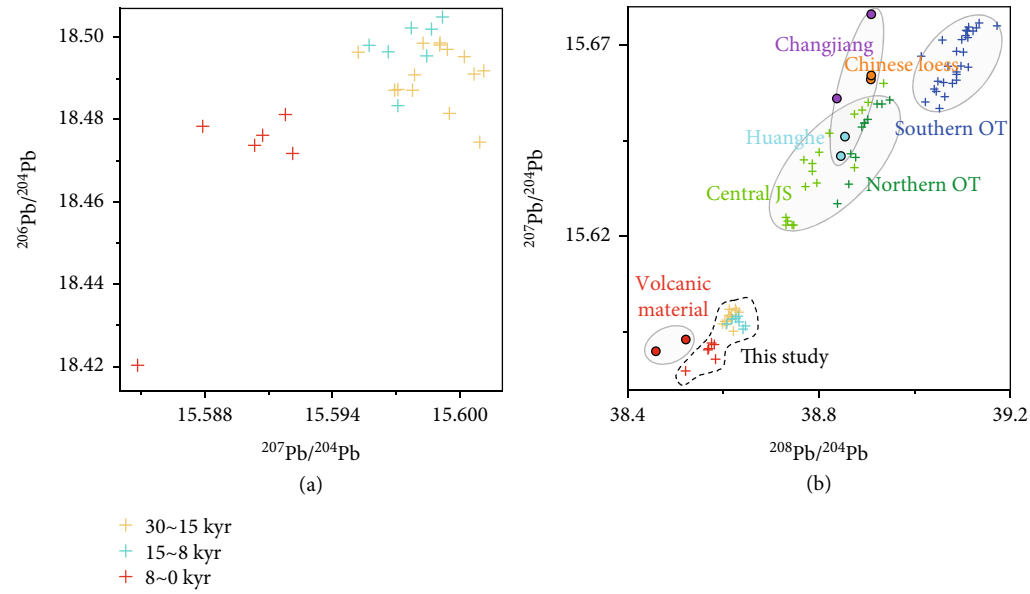

Figure 7: Sediment provenance discrimination diagrams of (a) $^{207}Pb/^{204}Pb$ vs. $^{206}Pb/^{204}Pb$ and (b) $^{208}Pb/^{204}Pb$ vs. $^{207}Pb/^{204}Pb$. Data of riverine sediments of the Changjiang River, Huanghe River, Japan Rivers, Chinese Loess Plaateau, and central JS come from [10]; the northern Okinawa Though [20] and southern Okinawa Though [67] are also shown for comparison.

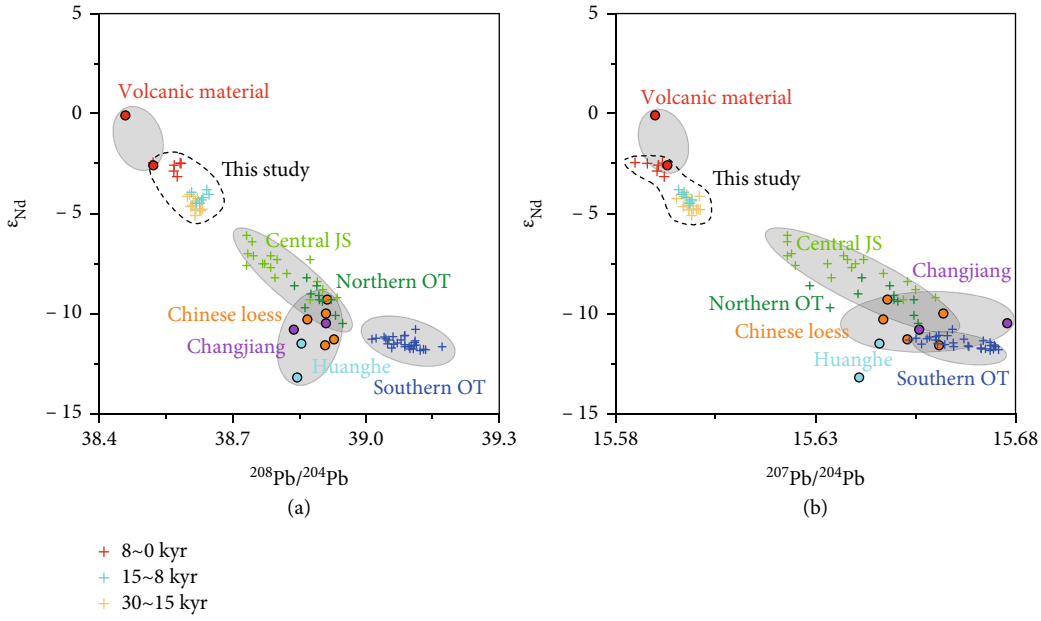

Figure 8: Sediment provenance discrimination diagrams of (a) $^{208}Pb/^{204}Pb$ vs. εNd and (b) $^{207}Pb/^{204}Pb$ vs. εNd. Data of riverine sediments of the Changjiang River, Huanghe River, Japan Rivers, and central JS come from [10]; the Chinese Loess Plateau data are from [10, 18]; the northern Okinawa Though [20] and southern Okinawa Though [67] are also shown for comparison.

intrude into the JS, increasing the overall heat content and melting sea ice in the western JS. This warming event was interrupted by subsequent HS1 cold event when cold water species of diatoms in the southern JS increased [64], TWC taxa sharply reduced [60], and perennial sea ice developed on the western coast of the JS [59].

The CIA of LV53-18-2 indicated that the study area had suffered weathering under a cold climate from 30 kyr to 15 kyr but fluctuated on a millennial timescale (Figure 10(g)). On the orbital timescale, this general upward trend of the CIA, indicating chemical weathering intensity, contradicts the weakened EASM (Figure 10(b)). We attributed this abnormal trend to source changes other than chemical weathering. Sea ice can carry weakly weathered large grain debris to the research area and distinctly affect sediment components, leading to lower CIA values. Therefore, the increase in the CIA index from 30 to 15 kyr can be explained by weakened sea ice activity.

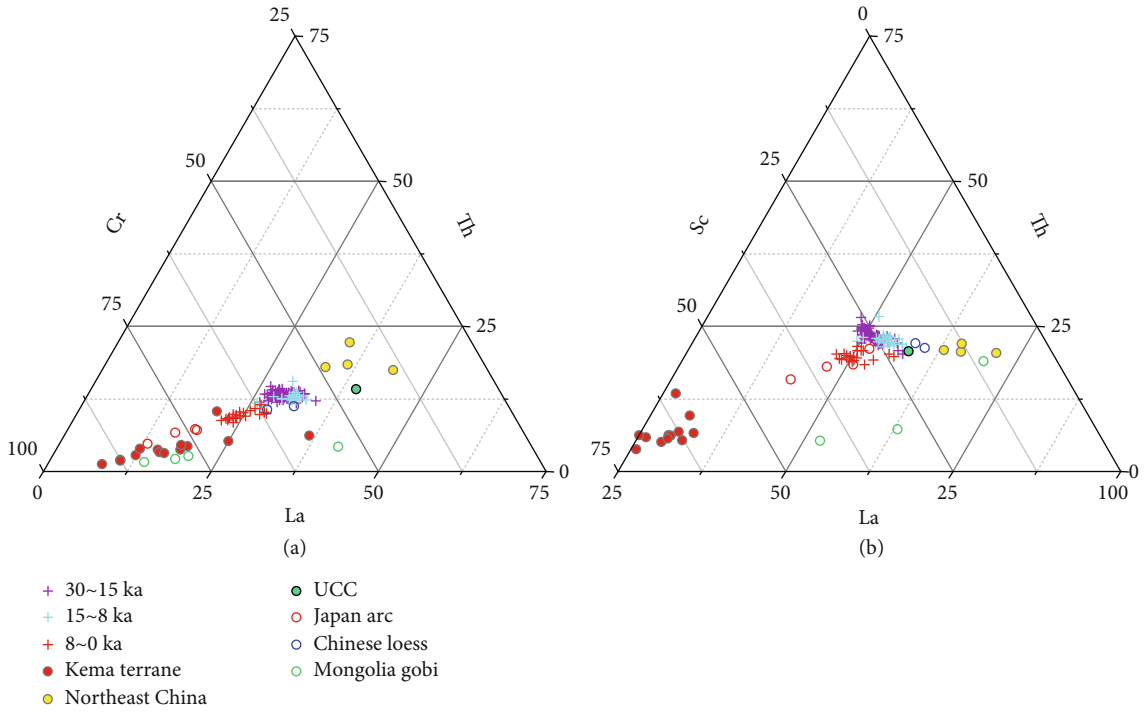

FIGURE 9: Provenance discrimination ternary plots of (a) La-Th-Cr and (b) La-Th-Sc. Data from the Kema terrane [44], northeast China [68], UCC [35], Japan arc [69], Chinese Loess Plateau [70], and Mongolian Gobi Desert [71] are also shown for comparison.

There are some fluctuations on the millennial timescale where the CIA index reaches a minimum, which can be explained by the input of a weakly weathered IRD. For instance, during the warming event at 19 kyr, deposition of a large quantity of IRD containing much large grain debris derived from the Far East coast influenced our core's Th/Sc ratio and led to smaller CIA values (Figures 10(e)–10(g)).

5.3.2. IRD Input from the Late Deglacial Period to the Early Holocene (15~8 kyr). The global climate began to warm up in pace with boreal summer insolation, increasing from 15 kyr [65]. The enhanced EASM, bringing more moisture and heat from low latitudes, has ameliorated the arid conditions of East Asia and reduced the source of dust generation [56]. However, the weakened Siberian High and temperature contrast between the polar and tropic region had diminished the loading ability of EAWM/WJ [6, 50]. The aeolian dust flux in the JS has reduced significantly since the late deglacial period [5].

Our Pb-Nd isotopic and ternary plots as well as the Sr-Nd discrimination plot [8] suggest that the provenance changed remarkably after 15 kyr. Furthermore, the La-Th-Sc and La-Th-Cr ternary plots show that the UCC provided more supply to this core during this period. Th/Sc ratio fluctuations show greater frequency and higher volatility than that during 30-15 kyr (Figure 10(f)). These changes can be attributed to IRD deposition. Figure 10(d) indicates that dramatic sea ice melting occurred from 15 kyr to 8 kyr in the research area. IRD deposition significantly alters sediment composition. Elemental evidence from our core indicates that sea ice transported more felsic debris to the study area during 15-8 kyr, although the source of the IRD is difficult to constrain due to the lithological complexity of coastal areas in the Far East.

A sharp decrease in the CIA index occurred at 15 kyr ago and first showed a downward and upward trend until about 8 kyr. Obviously, these variations are not in agreement with hemispheric warming on the orbital scale, which will enhance the weathering intensity and increase the CIA values, but are in harmony with the sea ice activity of our record. IRD deposition induced by intense sea ice melting remarkably affects the component, reduces the maturity of sediments, and causes insults in abnormally low CIA index from 15 to 8 kyr.

5.3.3. The Liman Cold Current since 8 kyr. The isotope and elemental tracing plots of our samples showed a notable increase in the contribution of mafic materials since 8 kyr. We suggest that the Kema terrane, which is the residual of the island arc on the western coast, is a the potential provenance. The EASM reached a maximum and then progressively declined from 8 kyr, and the WJ was much weaker than that in the glacial period. Therefore, the aeolian dust contribution to the JS was limited, as demonstrated in the southern and eastern cores [5]. In addition, the possibility of IRD input containing volcanic debris is unsupported by our data because of the weakening of sea ice activity after 8 kyr. As a result, current transportation is the only reasonable explanation.

The Liman Cold Current originates from the Tatar Strait and flows to the south along the western coast of the modern

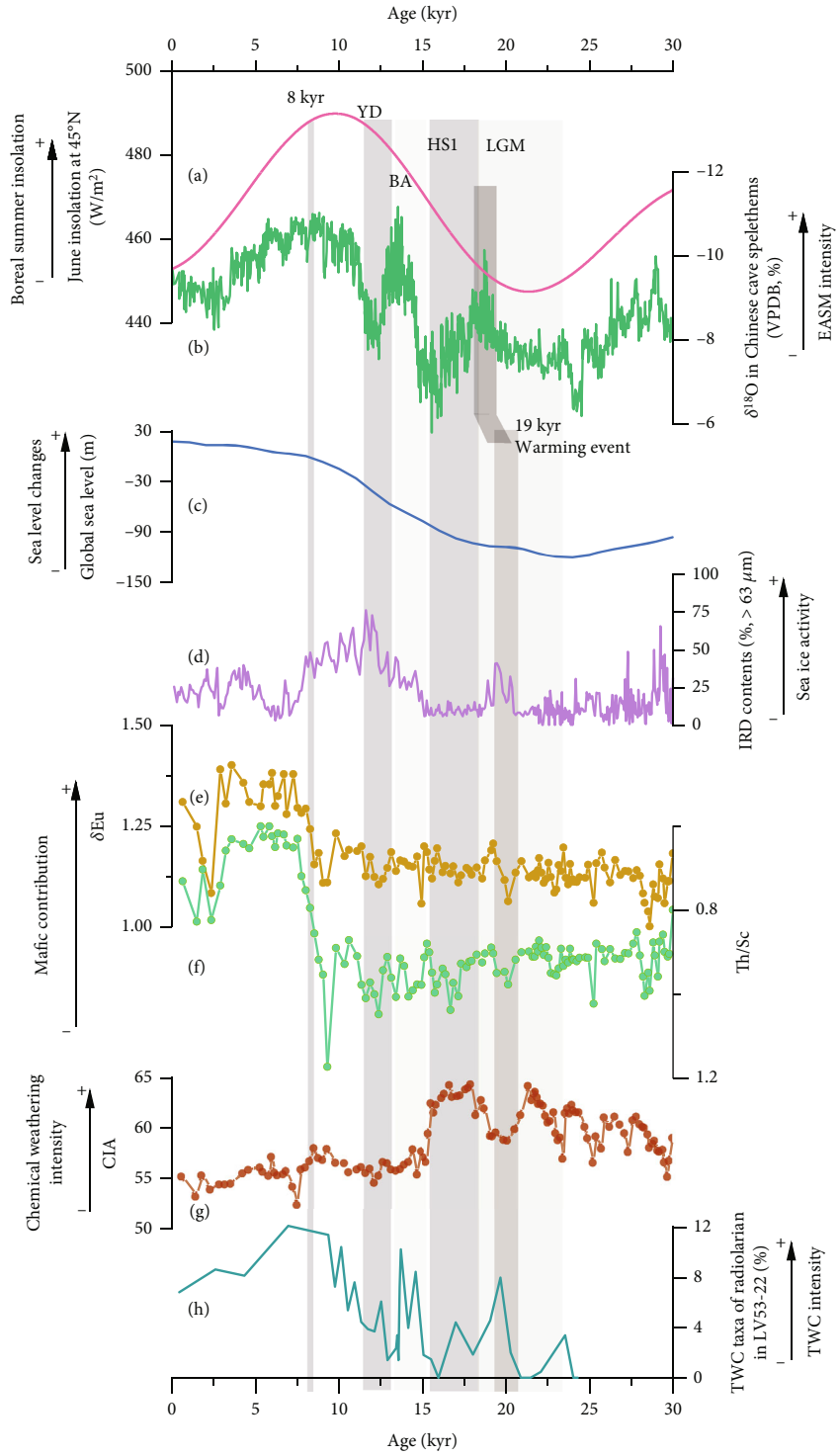

FIGURE 10: Comparison of global and regional records during the last glacial period. (a) June insolation at 45°N [49]; (b) Chinese speleothem $\delta^{18}O$ [63]; (c) global mean sea level [72]; (d) sea ice activity indicator of LV53-18-2 [59]; (e) and (f) proxies of the mafic contribution of LV53-18-2 [8]; (g) indicator of chemical weathering intensity of LV53-18-2 in this study; and (h) TWC intensity indicator of LV53-22 [60].

JS. The Amur River runoff is considered one of the primary sources of the LCC [28]. There are other scientific questions about the Tatar Strait and the LCC: When did the Tatar Strait open since the LGM, and is there any connection between the opening of the Tatar Strait and the birth of the LCC? Based on our elemental and isotopic results, we argue that (1) the Tatar Strait opened at about 8 kyr when the sea level continued to rise since the LGM and reached about -15 m, a height that opened the Tatar Strait. (2) Once the Tatar Strait opened, the freshwater input from the Amur River could cross the strait and give birth to the LCC, which could scour the coast upstream and bring mafic materials

from the Kema terrane to the study area, resulting in a δEu anomaly (Figure 10(e)) and a decrease in the Th/Sc ratio (Figure 10(f)).

During this period, the CIA index continued to decrease (Figure 10(g)). This is consistent with the fact that volcanic materials are generally rich in weakly weathered ash and glass. In this study, the CIA index was controlled by source variations, such as IRD or volcanic material, which eliminated the signal of chemical weathering induced by climate change.

6. Conclusion

We investigated the provenance variations of fine-grain terrigenous sediment in the western JS over the past 30 kyr based on major and trace element and Pb isotope from core LV53-18-2. Our results show that northeast China and the Kema terrane in the Far East are the two primary sources. During 30-15 kyr, the EAWM had carried dust from northeast China to the study area, and sea ice also transported weakly weathered IRD to deposition. From the late deglacial to the early Holocene (15-8 kyr), the deposition of large quantities of IRD remarkably influenced the nature of the sediments. After 8 kyr, more mafic materials derived from the Kema terrane were supplied to our core, supporting the deduction that the Tatar Strait opened and LCC generated at approximately 8 kyr due to rising sea levels. The CIA index of this core serves as an indicator of source changes, and not of chemical weathering intensity.

Data Availability

Data of this study can be available for all interested researchers upon request (zoujianjun@fio.org.cn; xfshi@fio.org.cn).

Conflicts of Interest

The authors declare that they have no conflict of interest regarding the publication of this article.

Authors' Contributions

JZ and XS conceived this study. AZ performed the measurements of sedimentary geochemistry. RD wrote the manuscript with input from JZ. All authors provided interpretation of results and comments on the manuscript and contributed to the manuscript.

Acknowledgments

We thank the ship crew and other participants for their assistance during cruise LV53. The funding for this research was supported by the National Natural Science Foundation of China (Grant Nos.: 41206059, 41420104005) and the Taishan Scholar Foundation of Shandong Province (TSQN20182117).

References

[1] T. Westerhold, N. Marwan, A. J. Drury et al., "An astronomically dated record of earth's climate and its predictability over the last 66 million years," *Science*, vol. 369, no. 6509, pp. 1383–1387, 2020.

[2] P. Wang, "Response of Western Pacific marginal seas to glacial cycles: paleoceanographic and sedimentological features," *Marine Geology*, vol. 156, no. 1–4, pp. 5–39, 1999.

[3] R. Tada, T. Irino, and I. Koizumi, "Land-ocean linkages over orbital and millennial timescales recorded in late Quaternary sediments of the Japan Sea," *Paleoceanography*, vol. 14, no. 2, pp. 236–247, 1999.

[4] R. Tada, T. Irino, K. Ikehara et al., "High-resolution and high-precision correlation of dark and light layers in the Quaternary hemipelagic sediments of the Japan Sea recovered during IODP expedition 346," *Progress in Earth and Planetary Science*, vol. 5, no. 1, 2018.

[5] K. Nagashima, R. Tada, H. Matsui, T. Irino, A. Tani, and S. Toyoda, "Orbital- and millenial-scale variations in asian dust transport path to the Japan Sea," *Palaeogeography Palaeoclimatology Palaeoecology*, vol. 247, no. 1-2, pp. 144–161, 2007.

[6] K. Nagashima, R. Tada, A. Tani et al., "Millennial-scale oscillations of the westerly jet path during the last glacial period," *Journal of Asian Earth Sciences*, vol. 40, no. 6, pp. 1214–1220, 2011.

[7] Z. Dong, X. Shi, C. Ge et al., "Evolution of westerly jet during the last 60 ka: evidence from core deposits in the central Japan (East) Sea," *Chinese Science Bulletin*, vol. 62, no. 11, pp. 1172–1184, 2017.

[8] R. Dou, J. Zou, X. Shi et al., "Geochemical and isotopic evidence for provenance of the Western Sea of Japan over the last 30000 years," *Frontiers in Earth Science*, vol. 9, 2021.

[9] J. Zou, X. Shi, A. Zhu et al., "Paleoenvironmental implications of Sr and Nd isotopes variability over the past 48 ka from the southern Sea of Japan," *Marine Geology*, vol. 432, article 106393, 2021.

[10] X. Shen, S. Wan, C. France-Lanord et al., "History of Asian eolian input to the Sea of Japan since 15 Ma: links to Tibetan uplift or global cooling?," *Earth and Planetary Science Letters*, vol. 474, pp. 296–308, 2017.

[11] W. Zhang, D. De Vleeschouwer, J. Shen, Z. Zhang, and L. Zeng, "Orbital time scale records of Asian eolian dust from the Sea of Japan since the early Pliocene," *Quaternary Science Reviews*, vol. 187, pp. 157–167, 2018.

[12] R. Tada, "Paleoceanographic evolution of the Japan Sea," *Palaeogeography, Palaeoclimatology, Palaeoecology*, vol. 108, no. 3-4, pp. 487–508, 1994.

[13] E. Garzanti, S. Andò, and G. Vezzoli, "Settling equivalence of detrital minerals and grain-size dependence of sediment composition," *Earth and Planetary Science Letters*, vol. 273, no. 1-2, pp. 138–151, 2008.

[14] S. M. Mclennan, S. R. Hemming, D. K. Mcdaniel, and G. N. Hanson, "Geochemical approaches to sedimentation, provenance, and tectonics," *Geological Society of America*, vol. 284, pp. 21–40, 1993.

[15] J. Chen, G. Li, J. Yang et al., "Nd and Sr isotopic characteristics of Chinese deserts: implications for the provenances of Asian dust," *Geochimica et Cosmochimica Acta*, vol. 71, no. 15, pp. 3904–3914, 2007.

[16] S. J. Goldstein and S. B. Jacobsen, "Nd and Sr isotopic systematics of river water suspended material: implications for crustal evolution," *Earth and Planetary Science Letters*, vol. 87, no. 3, pp. 249–265, 1988.

[17] S. M. McLennan, S. R. Taylor, M. T. McCulloch, and J. B. Maynard, "Geochemical and Nd-Sr isotopic composition of deep-sea turbidites: crustal evolution and plate tectonic associations," *Geochimica et Cosmochimica Acta*, vol. 54, no. 7, pp. 2015–2050, 1990.

[18] P. E. Biscaye, F. E. Grousset, M. Revel et al., "Asian provenance of glacial dust (stage 2) in the Greenland ice sheet project 2 ice Core, Summit, Greenland," *Greenland: Journal of Geophysical Research Oceans*, vol. 102, no. C12, pp. 26765–26781, 1997.

[19] J. Sun and X. Zhu, "Temporal variations in Pb isotopes and trace element concentrations within Chinese eolian deposits during the past 8Ma: implications for provenance change," *Earth and Planetary Science Letters*, vol. 290, no. 3-4, pp. 438–447, 2010.

[20] D. Zhao, S. Wan, S. Toucanne et al., "Distinct control mechanism of fine-grained sediments from Yellow River and Kyushu supply in the northern Okinawa Trough since the last glacial," *Geochemistry, Geophysics, Geosystems*, vol. 18, no. 8, pp. 2949–2969, 2017.

[21] L. Jolivet, K. Tamaki, and M. Fournier, "Japan Sea, opening history and mechanism: a synthesis," *Journal of Geophysical Research: Solid Earth*, vol. 99, no. B11, pp. 22237–22259, 1994.

[22] T. Oba, M. Kato, H. Kitazato et al., "Paleoenvironmental changes in the Japan Sea during the last 85, 000 years," *Paleoceanography*, vol. 6, no. 4, pp. 499–518, 1991.

[23] K. Kim, K. I. Chang, D. J. Kang, Y. H. Kim, and J. H. Lee, "Review of recent findings on the water masses and circulation in the East Sea (Sea of Japan)," *Journal of Oceanography*, vol. 64, no. 5, pp. 721–735, 2008.

[24] H. Che and J. Zhang, "Water mass analysis and end-member mixing contribution using coupled radiogenic Nd isotopes and nd concentrations: interaction between marginal seas and the northwestern Pacific," *Geophysical Research Letters*, vol. 45, no. 5, pp. 2388–2395, 2018.

[25] O. Katoh, K. Teshima, K. Kubota, and K. Tsukiyama, "Downstream transition of the Tsushima current west of Kyushu in summer," *Journal of Oceanography*, vol. 52, no. 1, pp. 93–108, 1996.

[26] K. A. Park, D. S. Ullman, K. Kim, J. Y. Chung, and K. R. Kim, "Spatial and temporal variability of satellite-observed subpolar front in the East/Japan Sea," *Deep Sea Research Part I Oceanographic Research Papers*, vol. 54, no. 4, pp. 453–470, 2007.

[27] S. Martin, E. Munoz, and R. Drucker, "The effect of severe storms on the ice cover of the northern Tatarskiy Strait," *Journal of Geophysical Research: Oceans*, vol. 97, no. C11, pp. 17753–17764, 1992.

[28] S. Martin and M. I. Kawase, "The southern flux of sea ice in the Tatarskiy Strait, Japan Sea and the generation of the Liman Current," *Journal of Marine Research*, vol. 56, no. 1, pp. 141–155, 1998.

[29] T. Gamo and Y. Horibe, "Abyssal circulation in the Japan Sea," *Journal of the Oceanographical Society of Japan*, vol. 39, no. 5, pp. 220–230, 1983.

[30] L. D. Talley, H. M. Dong, V. Lobanov, and V. A. Luchin, "Japan/East Sea water masses and their relation to the sea's circulation," *Oceanography*, vol. 19, no. 3, pp. 32–49, 2006.

[31] H. Sudo, "A note on the Japan Sea proper water," *Progress in Oceanography*, vol. 17, no. 3-4, pp. 313–336, 1986.

[32] Y.-I. Kumamoto, M. Yoneda, Y. Shibata et al., "Direct observation of the rapid turnover of the Japan Sea bottom water by means of AMS radiocarbon measurement," *Geophysical Research Letters*, vol. 25, no. 5, pp. 651–654, 1998.

[33] S. T. Yoon, K. I. Chang, S. Nam et al., "Re-initiation of bottom water formation in the East Sea (Japan Sea) in a warming world," *Scientific Reports*, vol. 8, no. 1, p. 1576, 2018.

[34] L. Yang, H. Long, L. Yi et al., "Luminescence dating of marine sediments from the Sea of Japan using quartz OSL and polymineral pIRIR signals of fine grains," *Quaternary Geochronology*, vol. 30, pp. 257–263, 2015.

[35] S. R. Taylor and S. M. McLennan, "The geochemical evolution of the continental crust," *Reviews of Geophysics*, vol. 33, no. 2, pp. 241–265, 1995.

[36] J. B. Mahoney, "Nd and Sr isotopic signatures of fine-grained clastic sediments: a case study of western Pacific marginal basins," *Sedimentary Geology*, vol. 182, no. 1-4, pp. 183–199, 2005.

[37] I. K. Um, M. S. Choi, J. J. Bahk, and J. H. Chun, "Provenance of late Quaternary sediments on the southwestern slope of the Ulleung Basin, East/Japan Sea," *Quaternary International*, vol. 459, pp. 153–164, 2017.

[38] Z. Xu, D. Lim, J. Choi, T. Li, S. Wan, and K. Rho, "Sediment provenance and paleoenvironmental change in the Ulleung Basin of the East (Japan) Sea during the last 21 kyr," *Journal of Asian Earth Sciences*, vol. 93, pp. 146–157, 2014.

[39] J. Zou, X. Shi, Y. Liu, J. Liu, K. Selvaraj, and S.-J. Kao, "Reconstruction of environmental changes using a multi-proxy approach in the Ulleung Basin (Sea of Japan) over the last 48 ka," *Journal of Quaternary Science*, vol. 27, no. 9, pp. 891–900, 2012.

[40] K. Nagashima, R. Tada, A. Tani, S. Toyoda, Y. Sun, and Y. Isozaki, "Contribution of aeolian dust in Japan Sea sediments estimated from ESR signal intensity and crystallinity of quartz," *Geochemistry Geophysics Geosystems*, vol. 8, no. 2, pp. 144–161, 2007.

[41] A. V. Lozhkin, P. M. Anderson, T. A. Brown, T. A. Grebennikova, J. A. Korzun, and V. I. Tsigankova, "Lake development and vegetation history in coastal Primor'ye: implications for Holocene climate of the southeastern Russian Far East," *Boreas*, vol. 50, no. 4, pp. 983–997, 2021.

[42] L. D. Talley, V. Lobanov, V. Ponomarev et al., "Deep convection and brine rejection in the Japan Sea," *Geophysical Research Letters*, vol. 30, no. 4, pp. 385–397, 2003.

[43] K. Ikehara, "Late Quaternary seasonal sea-ice history of the northeastern Japan Sea," *Journal of Oceanography*, vol. 59, no. 5, pp. 585–593, 2003.

[44] A. I. Malinovsky, V. V. Golozoubov, V. P. Simanenko, and L. F. Simanenko, "Kema terrane: a fragment of a back-arc basin of the early Cretaceous Moneron–Samarga island-arc system, East Sikhote–Alin range, Russian Far East," *Island Arc*, vol. 17, no. 3, pp. 285–304, 2008.

[45] A. I. Khanchuk, I. V. Kemkin, and N. N. Kruk, "The Sikhote-Alin orogenic belt, Russian South East: terranes and the formation of continental lithosphere based on geological and isotopic data," *Journal of Asian Earth Sciences*, vol. 120, pp. 117–138, 2016.

[46] A. V. Grebennikov, A. I. Khanchuk, V. G. Gonevchuk, and S. V. Kovalenko, "Cretaceous and Paleogene granitoid suites

of the Sikhote-Alin area (Far East Russia): geochemistry and tectonic implications," *Lithos*, vol. 261, pp. 250–261, 2016.

[47] S. Zaarur, M. Stein, O. Adam et al., "Synoptic stability and anomalies in NE China inferred from dust provenance of Sihailongwan maar sediments during the past ~80 kyr," *Quaternary Science Reviews*, vol. 239, article 106279, 2020.

[48] H. W. Nesbitt and G. M. Young, "Early Proterozoic climates and plate motions inferred from major element chemistry of lutites," *Nature*, vol. 299, no. 5885, pp. 715–717, 1982.

[49] A. Berger and M. F. Loutre, "Insolation values for the climate of the last 10 million years," *Quaternary Science Reviews*, vol. 10, no. 4, pp. 297–317, 1991.

[50] Y. Sun, S. C. Clemens, C. Morrill, X. Lin, X. Wang, and Z. An, "Influence of Atlantic meridional overturning circulation on the East Asian winter monsoon," *Nature Geoscience*, vol. 5, no. 1, pp. 46–49, 2012.

[51] Y. J. Wang, H. Cheng, R. L. Edwards, Z. S. An, J. Y. Wu, and J. A. Dorale, "A high-resolution absolute-dated Late Pleistocene monsoon record from Hulu Cave, China," *Science*, vol. 294, no. 5550, pp. 2345–2348, 2001.

[52] T. Oba and T. Irino, "Sea level at the last glacial maximum, constrained by oxygen isotopic curves of planktonic foraminifera in the Japan Sea," *Journal of Quaternary Science*, vol. 27, no. 9, pp. 941–947, 2012.

[53] Z. Dong, X. Shi, J. Zou et al., "Paleoceanographic insights on meridional ventilation variations in the Japan Sea since the last glacial maximum: a radiolarian assemblage perspective," *Global and Planetary Change*, vol. 200, article 103456, 2021.

[54] S. A. Gorbarenko and J. R. Southon, "Detailed Japan Sea paleoceanography during the last 25 kyr: constraints from AMS dating and δ18O of planktonic foraminifera," *Palaeogeography Palaeoclimatology Palaeoecology*, vol. 156, no. 3-4, pp. 177–193, 2000.

[55] Y. Wu, X. Shi, X. Gong et al., "Evolution of the upper ocean stratification in the Japan Sea since the last glacial," *Geophysical Research Letters*, vol. 47, no. 16, 2020.

[56] S. Yang, X. Dong, and J. Xiao, "The east Asian monsoon since the last glacial maximum: evidence from geological records in northern China," *Science China Earth Sciences*, vol. 62, pp. 1169–1181, 2019.

[57] T. Irino and R. Tada, "High-resolution reconstruction of variation in aeolian dust (Kosa) deposition at ODP site 797, the Japan Sea, during the last 200 ka," *Global and Planetary Change*, vol. 35, no. 1-2, pp. 143–156, 2003.

[58] K. Ikehara and K. Fujine, "Fluctuations in the late Quaternary East Asian winter monsoon recorded in sediment records of surface water cooling in the northern Japan Sea," *Journal of Quaternary Science*, vol. 27, no. 9, pp. 866–872, 2012.

[59] R. Dou, J. Zou, X. Shi et al., "Reconstructed changes in sea ice in the western Sea of Japan over the last 30, 000 years," *Quaternary Sciences*, vol. 40, no. 3, pp. 690–703, 2020.

[60] Z. Dong, X. Shi, J. Zou et al., "Drastic hydrographic changes inferred from radiolarian assemblages in the central Japan Sea since the last glacial maximum," *Marine Geology*, vol. 429, article 106295, 2020.

[61] E. Monnin, A. Indermühle, A. Dällenbach et al., "Atmospheric CO2 Concentrations over the last glacial termination," *Science*, vol. 291, no. 5501, pp. 112–114, 2001.

[62] J. P. Liu, J. D. Milliman, S. Gao, and P. Cheng, "Holocene development of the Yellow River's subaqueous delta, North Yellow Sea," *Marine Geology*, vol. 209, no. 1-4, pp. 45–67, 2004.

[63] H. Cheng, R. L. Edwards, A. Sinha et al., "The Asian monsoon over the past 640, 000 years and ice age terminations," *Nature*, vol. 534, no. 7609, pp. 640–646, 2016.

[64] I. Koizumi, R. Tada, H. Narita et al., "Paleoceanographic history around the Tsugaru Strait between the Japan Sea and the Northwest Pacific Ocean since 30 cal kyr BP," *Palaeogeography, Palaeoclimatology, Palaeoecology*, vol. 232, no. 1, pp. 36–52, 2006.

[65] G. H. Denton, R. F. Anderson, J. R. Toggweiler, R. L. Edwards, J. M. Schaefer, and A. E. Putnam, "The last glacial termination," *Science*, vol. 328, no. 5986, pp. 1652–1656, 2010.

[66] X. Shi, J. Zou, Z. Yao, and R. Dou, "Sedimentation and environment evolution of the Sea of Japan since the last glaciation and its driving forces," *Marine Geology & Quaternary Geology*, vol. 39, no. 3, 2019.

[67] Y. Dou, S. Yang, X. Shi et al., "Provenance weathering and erosion records in southern Okinawa Trough sediments since 28 ka: geochemical and Sr–Nd–Pb isotopic evidences," *Chemical Geology*, vol. 425, pp. 93–109, 2016.

[68] Y. Xie, C. Kang, Y. Chi, H. Du, J. Wang, and L. Sun, "The loess deposits in Northeast China: the linkage of loess accumulation and geomorphic-climatic features at the easternmost edge of the Eurasian loess belt," *Journal of Asian Earth Sciences*, vol. 181, article 103914, 2019.

[69] S. Togashi, N. Imai, Y. Okuyama-Kusunose et al., "Young upper crustal chemical composition of the orogenic Japan arc," *Geochemistry, Geophysics, Geosystems*, vol. 1, no. 11, 2000.

[70] B.-M. Jahn, S. Gallet, and J. Han, "Geochemistry of the Xining, Xifeng and Jixian sections, Loess Plateau of China: eolian dust provenance and paleosol evolution during the last 140 ka," *Chemical Geology*, vol. 178, no. 1-4, pp. 71–94, 2001.

[71] B. A. Maher, T. J. Mutch, and D. Cunningham, "Magnetic and geochemical characteristics of Gobi Desert surface sediments: implications for provenance of the Chinese Loess Plateau," *Geology*, vol. 37, no. 3, pp. 279–282, 2009.

[72] R. M. Spratt and L. E. Lisiecki, "A Late Pleistocene sea level stack," *Climate of the Past*, vol. 12, no. 4, pp. 1079–1092, 2016.